Crystallization kinetics of suspensions of hard colloidal spheres

J. L. Harland and W. van Megen*
Department of Applied Physics, Royal Melbourne Institute of Technology, Melbourne, Victoria 3000, Australia
(Received 27 June 1996; revised manuscript received 4 November 1996)

The crystallization of suspensions of sterically stabilized polymer particles, with hard-sphere-like interactions, is studied by laser light scattering. Over the range of volume fractions examined, from just below melting to the glass transition, crystallization occurs by homogeneous nucleation. After the suspensions are shear melted, the intensity, position, and width of the main interlayer Bragg reflection are measured as functions of time. From these the amount of crystal, the average linear crystal dimension, the number of crystals, and the volume fraction of the crystal phase are obtained. No assumptions are made concerning the functional time dependence of nucleation or growth processes. Below the melting concentration the observed crystallization process is compatible with the classical picture of sequential nucleation and growth of isolated crystals. However, when the melting concentration is exceeded, nucleation events are correlated, nucleation is accelerated, and high nucleation rate densities suppress crystal growth. Above the melting concentration we infer, with the aid of the equations of state for the hard-sphere fluid and solid, that the first identifiable crystals are in mechanical equilibrium with the embedding fluid and, consequently, strongly compressed by it. Ensuing nucleation lags expansion of the crystal lattice. [S1063-651X(97)12302-9]

PACS number(s): 82.70.Dd, 64.70.Dv, 81.10.Fq

I. INTRODUCTION

Colloidal suspensions of hard polymer particles show a freezing-melting transition, as well as a glass transition, similar to those expected for a perfect hard-sphere system. At suspension concentrations that lie between the freezing and glass transitions, crystallization occurs by homogeneous nucleation. In this paper we describe time-resolved light-scattering studies of this crystallization process.

The motivation for studies of the dynamical properties of model colloidal suspensions is not only to provide a better understanding of the suspensions, but also for its potential generic value. There is a formal equivalence of the thermodynamic properties between an atomic system and a suspension of particles having the same interaction potentials [1]. However, on the time scale of interparticle collisions, the motions of suspended particles are diffusive rather than ballistic, as is the case for atomic systems. Despite this fundamental difference in their respective small-scale motions, studies of large-scale particle motions [1,2] and crystal growth [3] indicate clear analogies in the dynamical properties between suspensions and atomic systems.

Transformation of an undercooled fluid to the crystal phase remains one of the more interesting aspects of condensed-matter science. An experimental determination of the mechanisms of solidification of atomic or molecular fluids is severely hindered by very high crystallization rates, particularly at significant undercooling, slow dissipation of latent heat, and the domination of heterogeneous nucleation due to impurities and container walls [4]. Furthermore, a complete theoretical treatment of crystallization of a molecular fluid, taking into account the coupling among the nonconserved order parameter and the five conserved fields (energy, density, and the momentum components), has so far proved intractable. Understandably, the classical theory of solidification [5], formulated some 50 years ago, still dominates our current view. The basic version of this theory proposes that isolated sharply defined spherical crystal nuclei form spontaneously by thermally driven density fluctuations, but that the energy barrier posed by competing bulk and surface contributions results in the survival of only those nuclei that exceed a minimum (critical) radius. In the absence of seeding, liquids can be cooled below their freezing temperatures without crystallization, but deeply quenched liquids crystallize almost instantly. These observations support the notion of large nucleation barriers at slight undercoolings and small barriers at large undercoolings. They also suggest, as is borne out by experiments to date, that it is exceedingly difficult, if not impossible, to resolve the nucleation and growth processes and determine their respective time dependencies under the same experimental conditions [4].

Crystallization of colloidal suspensions presents a more tractable problem in terms of both theoretical description and experimental resolution. Suspensions of ''model'' particles, spheres [6], or rods [7] with narrow size and shape distributions, and certain mixtures of spheres [8], crystallize on accessible time scales, typically ten orders of magnitude slower than is the case for deeply quenched molecular liquids. The continuous suspending medium acts as an effective thermal sink. In addition, laboratory samples are sufficiently small and free from impurities that heterogeneous nucleation is avoided. Slow crystallization rates, combined with the weak lattice forces of colloidal crystals, allow studies of the structure and particle dynamics of metastable colloidal fluids and glasses [9], as well as the kinetics of crystallization. It should also be mentioned that phase transitions in these suspensions occur at constant volume, rather than constant pressure, and the particle volume fraction or concentration is the only control parameter. Temperature plays no (direct) role. Accordingly, freezing and melting *concentrations* are identified.

*Author to whom correspondence should be addressed.

Given the slow crystallization of suspensions and the fact that the crystals can be detected with visible light, several different but complementary experimental procedures for measuring crystallization kinetics present themselves. Direct observation or video microscopy, low-angle laser light scattering (which measures the development of particle concentration difference between the growing crystals and the embedding fluid), and scattering from one or more sets of crystal planes (the light scattering equivalent of x-ray powder diffraction), have been applied to suspensions of charge-stabilized and sterically stabilized (hard-sphere-like) particles. The drawbacks and attributes of each of these techniques were recently reviewed by Schätzel [10].

These studies show different crystal growth processes. In the case of suspensions of particles with long-ranged screened Coulomb interactions, the crystal size is found to increase linearly with time [3] whereas, for particles with hard-sphere-like interactions, the size increases with the square root in time [11]. For the hard-sphere system the difference in the number densities of coexisting crystal and fluid phases is appreciable, and the observed nonlinear crystal growth laws have been explained by the coupling of the (nonconserved) order parameter to the number density which, in the case of large attachment efficiencies, leads to diffusion-limited growth [12]. These and other studies [13,14] have enhanced understanding of crystal growth. However, because constant nucleation rates were generally assumed in these works, they have not clarified the time dependence of the nucleation process nor the extent to which nucleation and growth compete.

In this paper we describe measurements of the growth of the main Bragg peak during the crystallization of nonaqueous suspensions of sterically stabilized polymer particles. The size, number, and density of the crystals are calculated from the intensity of the peak, its width, and position. In principle no assumptions concerning the nature of the time dependencies of the growth or nucleation rates are necessary. One of the main observations of this work is an apparent change in crystallization mechanism when the melting concentration is exceeded. Below melting, the observed crystallization is compatible with the classical picture of the formation of isolated nuclei followed by growth. Above the melting concentration, crystal growth of any significance appears to be suppressed by very high nucleation rates. Moreover, as outlined in a preceding Letter [15], nucleation in very concentrated suspensions is accelerated rather than constant.

In Sec. II we describe the suspension and its phase behavior, the experimental arrangement, and the analysis employed to obtain the moments of the main Bragg reflection. Results are presented in Sec. III followed by their discussion in Sec. IV. Concluding remarks are presented in Sec. V.

II. EXPERIMENT

A. Sample description

The preparation and characteristics of the suspensions used in this work have been described previously [16]. Briefly, the particles comprise spherical cores of poly(methyl methacrylate) (PMMA), sterically stabilized by chemically grafted surface layers of poly(12-hydroxystearic acid) (PHSA) about 10 nm thick. The particles were suspended in a liquid mixture of decalin and carbon disulfide, the relative amounts of which were adjusted until the suspension's turbidity fell below about 0.05 cm^{-1}. Thus, when viewed in 1-cm path-length cells, the suspensions were virtually transparent and, therefore, suitable for light scattering studies even at particle concentrations up to close packing. The average hydrodynamic radius $R_h = 200 \pm 2$ nm and polydisperity $\sigma \approx 5\%$ of the particles were measured by dynamic light scattering on very dilute samples [17].

Rather than a temperature quench, the usual first step in crystallization experiments with molecular systems [4], a quenched (metastable) state of a colloidal suspension is prepared by shaking or tumbling a sample. That such tumbling action effectively randomizes the particle positions is then evident from the amorphous appearance of the sample as well as the fluidlike shape of its static structure factor [18].

As described elsewhere [6], the phase behavior of these suspensions mimics that of the hard-sphere system. Freezing and melting concentrations are respectively identified as the concentration where crystallization first occurs and that where the suspension becomes fully crystalline. Equating the observed freezing concentration with the value, $\phi_f = 0.494$, known for the freezing volume fraction of hard spheres [19], gives a multiplicative factor with which concentrations of all samples can be converted to effective hard-sphere volume fractions, ϕ. Importantly, the observed effective hard-sphere volume fraction at melting, $\phi_m = 0.545 \pm 0.003$, agrees with that expected for perfect hard spheres [19], implying that the particle interactions can be regarded as hard-sphere-like. Measurements of diffusion coefficients and sedimentation velocities on similar PHSA-stabilized PMMA suspensions support this inference [16,20]. The effective hard-sphere particle radius, $R = 201 \pm 1$ nm, was obtained from the measured value q_s, and the value $q_s R = 3.47$ predicted for the position of the primary maximum of the structure factor of the (hard sphere) fluid at freezing [21]. Note that, aside from experimental errors, the hydrodynamic and effective hard-sphere radii are the same, and in the following discussion we use the value $R = 201$ nm for the particle radius.

The shear-melted metastable fluid is easily recovered from the crystallized colloid by tumbling the sample. Homogeneously nucleated crystallization occurs in suspensions with concentration up to $\phi_g \approx 0.58$. This is evident from the appearance, usually within about 30 min, of small Bragg reflecting crystals randomly distributed throughout the sample. Interestingly, the concentration ϕ_g coincides with the value where, in the metastable colloidal fluid, large-scale particle diffusion ceases [9,22]. Accordingly, ϕ_g is identified as the glass transition concentration. Suspensions with concentrations greater than ϕ_g still crystallize, at least partially, by the slow growth of large and irregularly shaped crystals on secondary nuclei, such as the container walls and regions of shear-aligned structures remaining from the tumbling action [23]. In this work we study the crystallization of nine samples in the concentration range 0.530–0.575, as listed in Table I.

B. Light scattering

Figure 1 shows a schematic diagram of the spectrometer used. It consists of a cylindrical thermostatted sample holder

TABLE I. Sample designation (column 1), suspension volume fraction, ϕ, initial and final volume fractions of the crystal phase, $\phi_c(0)$ and $\phi_c(t_f)$, and fluid phase, $\phi_l(0)$ and $\phi_l(t_f)$. Uncertainties in the stated volume fractions are about ± 0.002.

Sample	ϕ	$\phi_c(t=0)$	$\phi_c(t_f)$	$\phi_l(t=0)$	$\phi_l(t_f)$
*J*0	0.530	0.558	0.552	0.503	0.498
*J*1	0.537	0.573	0.554	0.515	0.500
*J*2	0.548	0.598	0.564	0.538	0.508
*J*3	0.553	0.609	0.570	0.549	0.513
*J*4	0.557	0.611	0.574	0.551	0.516
*J*5	0.561	0.619	0.580	0.559	0.521
*J*6	0.565	0.623	0.583	0.564	0.524
*J*7	0.570	0.628	0.590	0.569	0.531
*J*8	0.575	0.631	0.599	0.573	0.539

containing a liquid (a mixture of decalin and tetralin) having the same refractive index ($n=1.501\pm0.001$) as the suspension. A glass cell, of 10-mm-square cross section and 30 mm in height, containing the suspension is mounted along the axis of the sample holder and illuminated by a 3-mW diode laser beam (wavelength=678.7 nm), expanded and collimated to 8-mm square cross section. The sample holder focuses the scattered light to a vertical line which is then focused to a point on the detector by a cylindrical lens positioned with its axis perpendicular to that of the sample holder. The detector, an Oriel Instaspec III Diode Array Camera, consisting of a linear array of 512 diodes over a length of 12.8 mm, is mounted on a goniometer rotating on the axis of the sample holder. Computer control of the goniometer and detector allow data collection at preset angles and time intervals.

With the above arrangement, intensities $I(q;t)$ were measured over a range of scattering vectors, Δq, such that $\Delta q/q_m \approx 0.1$, centered on the position q_m of the main Bragg reflection. The overall resolution $\delta q/q_m$ was about 0.0005. A given sample was prepared by tumbling it for several hours on a rotary suspension mixer. It was then immediately placed in the spectrometer (defining $t=0$) and data sets $I(q;t)$ collected at predetermined times, t, up to $t_f=20$ h. This process was repeated five times for each sample.

C. Data analysis

Large numbers of apparently randomly oriented crystals in the scattering volume should give a reasonable estimate of the orientationally averaged diffraction pattern. Previous work [24] has shown that the lowest-lying features of this diffraction pattern, which consist of a sharp Bragg reflection superimposed on a much broader peak, result from a random stacking of close-packed layers of particles. However, this random stacking along with scattering from any uncrystallized suspension and the difficulty of estimating the single-particle form factor all mitigate accurate isolation of one or more of the Bragg reflections, particularly during the early stages of the crystallization at low concentrations ($\phi \gtrsim \phi_f$). First, the random stacking smears out all reflections aside from those common to both fcc and hcp structures. Second, all but the lowest interlayer reflection ({111} in fcc indexing) tend to be weakened by the particle form factor $P(q)$. In addition, the main fluid structure factor peak and the smeared {200} reflection have roughly the same location as the interlayer reflection. Third, the close matching of the refractive indices of the suspending liquid mixture and the particles effectively precludes measurement of $P(q)$ with sufficient accuracy to calculate the structure factor $S(q;t)$, directly from $I(q;t)/P(q)$. Notwithstanding these difficulties, we isolate the growth of the {111} reflection by the following procedures.

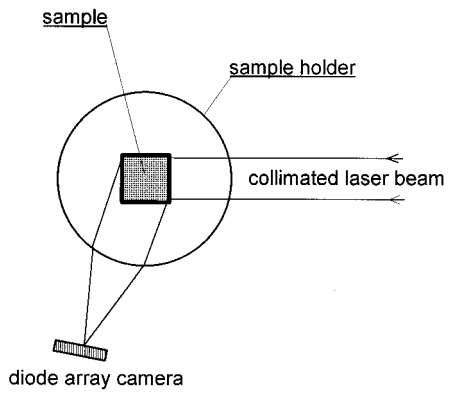

FIG. 1. Schematic illustration of the spectrometer.

Previous work [18] with suspensions similar to those used here has shown that, in the region of q_m, the static structure factor of the metastable colloidal fluids can be described quite accurately by the Percus-Yevick result $S_{\mathrm{PY}}(q)$ for the hard-sphere fluid. Accordingly, we estimate the particle form factor $\alpha P(q)$ in arbitrary units, by dividing the intensity $I(q;0)$, measured immediately after shear melting, by $S_{\mathrm{PY}}(q)$ at the hard-sphere volume fraction corresponding to that of the sample, i.e.,

$$\alpha P(q) = I(q;0)/S_{\mathrm{PY}}(q). \tag{1}$$

The contrast factor α varied from sample to sample, presumably due to small variations in the CS_2 to decalin ratio. The structure factor $S(q;t)$ (again in arbitrary units) of the crystallizing suspension is then obtained (for $t>0$) from

$$S(q;t) = I(q;t)/\alpha P(q). \tag{2}$$

The quantity $S(q;t)$ represents the structure factor of colloidal crystal plus fluid over the range of scattering vectors spanned by the detector. From this the Bragg peak is isolated

between scattering vectors q_1 and q_2 (see Fig. 3) as follows. To subtract the fluid contribution to $S(q;t)$ the scale factor $\beta(t)$ is increased until the function $\beta(t)S_{\rm PY}(q)$ first comes into contact with $S(q;t)$. The scattering vector q_1, where this occurs, defines one extremity of the Bragg peak. The other extremity q_2 is chosen where $S(q;t)-\beta(t)S_{\rm PY}(q)$ is a minimum. The instantaneous Bragg peak $S_c(q;t)$ $(q_1 \leqslant q \leqslant q_2)$ is then calculated from

$$S_c(q;t)=S(q;t)-\beta(t)S_{\rm PY}(q). \tag{3}$$

Here we assume that the diffuse scattering, due to random stacking plus the scattering from the remaining fluid, can be described by $S_{\rm PY}(q)$. One can see from Fig. 1 of Ref. [24] that the broadband of diffuse scattering from the crystal has a similar shape to the fluid's main structure factor peak.

From the Bragg peak $S_c(q;t)$, the position $q_m(t)$ of its maximum, and its width $\Delta q(t)$ at half maximum, the following quantities are obtained. First, the fraction $X(t)$ of the sample converted from fluid to crystal is calculated from [10]

$$X(t)=c\int_{q_1}^{q_2} S_c(q;t)dq, \tag{4}$$

where the constant c is chosen such that $X(t_f)=1$ at the melting concentration ($t_f=20$ h is the duration of the measurement). Once $X(t)>0.03$, we find that $X(t)$ and the other moments of $S_c(t)$, defined below, are insensitive to the width of the integration window, used in Eq. (4), and to whether $\beta S_{\rm PY}(q)$ or simply a constant is chosen to subtract the effects of the scattering from the fluid.

Second, the average linear crystal dimension (in units of the particle diameter $2R$) is given by [25]

$$L(t)=\pi K/\Delta q(t)R, \tag{5}$$

where $K=1.155$ is the Scherrer constant for a crystal of cubic shape.

Third, the number density of (average-sized) crystals is

$$N_c(t)=X(t)/L^3(t), \tag{6}$$

and the rate of addition of crystals, which we shall identify as the nucleation rate density, is given by $R_c(t)=dN_c(t)/dt$.

Fourth, it is easily shown that the volume fraction $\phi_c(t)$ of a fcc crystal is related to the location $q_m(t)$ of the {111} reflection as follows:

$$\phi_c(t)=\frac{2}{9\pi^2\sqrt{3}}\,(q_m(t)R)^3. \tag{7}$$

Since the volume fraction of structures of close-packed planes is independent of the stacking arrangement, we interpret $\phi_c(t)$ as the average volume fraction of the crystal phase, which we assume to consist of close-packed planes with reciprocal spacing $q_m(t)$.

Finally, the volume fraction $\phi_l(t)$ of the colloidal fluid in mechanical equilibrium with the crystal is calculated with the aid of the equations of state established from computer simulations for the hard-sphere fluid [26] and crystal [27]. Then, assuming mechanical equilibrium between crystal and fluid phases to hold during the course of crystallization, we obtain another estimate of the fraction, $X^*(t)$, of crystal in the sample from the requirement

$$\phi=X^*(t)\,\phi_c(t)+(1-X^*(t))\,\phi_l(t). \tag{8}$$

III. RESULTS

In the following presentation and discussion of the data, all lengths are expressed in units of the particle diameter $(2R)$ and times in units of the Brownian characteristic time, $\tau_b=R^2/D_0$ $(=0.047$ s), where D_0 is the free-particle diffusion constant. We also introduce the (dimensionless) interaction time $\tau_I=D^{-1}$, where $D=D(\phi)$ is the long-time single-particle diffusion coefficient in units of D_0. $\tau_I=\tau_I(\phi)$ represents the time taken for a particle to diffuse a distance equal to its radius.

The quantities defined in Eqs. 4–7 were determined for suspensions at concentrations listed in Table I. In Fig. 2 we show the intensities $I(q;t)$ spanning the detector window during the early and most rapid stage of crystallization for a suspension below [$\phi=0.537$, Fig. 2(a)] and for one above [$\phi=0.557$, Fig. 2(b)] the melting concentration ϕ_m. The basic features are preserved after form factor division (Fig. 3), according to Eqs. (1) and (2), and subtraction of the fluid structure (Fig. 4) according to Eq. (3). The scattering vectors q_1 and q_2 bracketing the Bragg peak are also indicated in Fig. 3. The obvious difference between the widths of the emerging peaks, seen for the two suspension concentrations, reflects the respective difference in average crystal size. Shifts in the positions of the peaks to lower scattering vectors, indicating expansion of the crystal lattice, are seen to accompany increases in peak intensities.

Figure 5 shows a typical result for the fraction of crystal, calculated from the area under the Bragg peak by Eq. (4), as a function of time, at the suspension concentration $\phi=0.548$. As in other work [11,14], the initial fast rate of conversion from colloidal fluid to crystal is attributed to nucleation and growth, and the slower rate of conversion, seen at longer times, to coarsening. The procedures by which the induction time $\tau_{\rm ind}$ and crossover time $\tau_{\rm cross}$ are determined are also indicated in Fig. 5. These times are shown as functions of the suspension concentration in Fig. 6.

The broad dynamic range of the crystal growth process is illustrated more clearly in plots of $\log_{10}[X(\tau)]$ versus $\log_{10}[\tau]$ shown in Fig. 7. The overall rate of conversion increases as the suspension concentration is increased from 0.530 to about 0.55 [Fig. 7(a)], and then decreases with further increase of the concentration to 0.575 [Fig. 7(b)]. Note also that, with increasing concentration, the interval where $X(\tau)$ increases most rapidly is preceded by a stage of progressively slower conversion which becomes sublinear in time as the glass transition ($\phi_g \approx 0.58$) is approached. Power-law exponents μ, shown in Fig. 8, were obtained from the slopes of straight lines fitted to the steepest sections of the $\log_{10}[X(\tau)]$ versus $\log_{10}[\tau]$ plots of Fig. 7.

In Fig. 9 we compare, for a suspension from the middle of the range of sample concentrations, the fraction of crystal, $X(\tau)$, calculated from Eq. (4), with that obtained from

$$X(\tau)=2c\int_{q_m}^{q_2} S_c(q;\tau)dq. \tag{9}$$

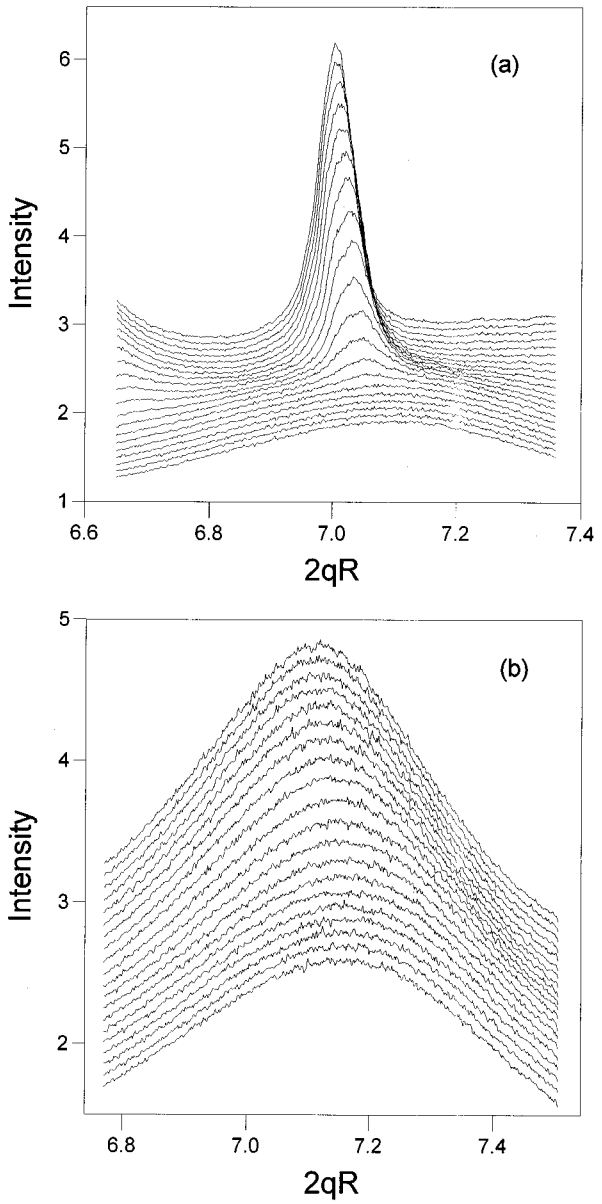

FIG. 2. Intensities in arbitrary units vs the (dimensionless) scattering vector $2qR$ shown at 20-s intervals. Consecutive data sets are displaced by 0.08 units. Data are shown for (a) $\phi=0.537$ and (b) $\phi=0.557$.

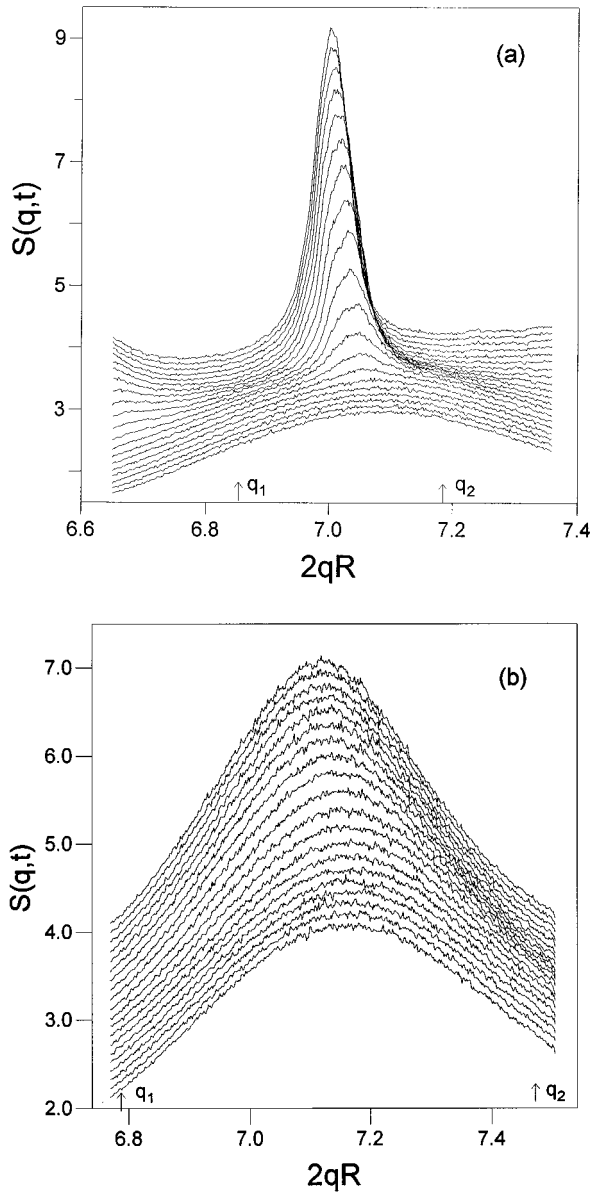

FIG. 3. As in Fig. 2, but now showing total structure factors, in arbitrary units, obtained after division of intensities by particle form factors. The window used in the calculation of the moments of the peak is bracketed by q_1 and q_2. See text for further description.

The agreement between the two estimates of the fraction of crystal occupying the sample volume indicates that any asymmetry of the Bragg peak about q_m has a negligible effect. In Fig. 9 we also show the complement $1-\beta(\tau)$ of the amplitude of the fluid structure factor $S_{\mathrm{PY}}(q)$ subtracted from the total structure factor $S(q;t)$ [in Eq. (3)], to yield the structure factor $S_c(q;t)$ of the crystal phase. Assuming that, during the course of conversion of fluid to crystal, the reduction of light scattered by the fluid is proportional to the increase in intensity of the {111} reflection and the increase in diffuse scattering due to random stacking, then $1-\beta(\tau)$ represents another measure of the fraction of the sample occupied by crystal. Note that β and X have been normalized such that $\beta(0)=1$ and, for a sample that is fully crystallized, $X(t_f)=1$. Aside from random differences at short times, $X(\tau)$ and $1-\beta(\tau)$ are proportional, giving further support to the procedure, described in Sec. II C, used to isolate the Bragg peak. The constant multiplicative difference of about 10 between $X(\tau)$ and $1-\beta(\tau)$ indicates that most of the ''background'' subtracted, in Eq. (3), is diffuse scattering resulting from the random stacking of close-packed layers rather than scattering from the fluid.

The average linear crystal dimensions $L(\tau)$ calculated from the peak widths via Eq. (5), are shown in Fig. 10. For the lowest two suspension concentrations ($\phi=0.530$ and 0.537) the data suffer from considerable statistical uncertainties, particularly at early times, due to poor orientational averaging over small numbers of crystals in the illuminated region. Consequently, it is not possible to specify power-law growth-rate exponents in these cases. Nonetheless, one can see that $L(\tau)$ has increased significantly over the same time interval where $X(\tau)$, in Fig. 7(a), shows its strongest rate of

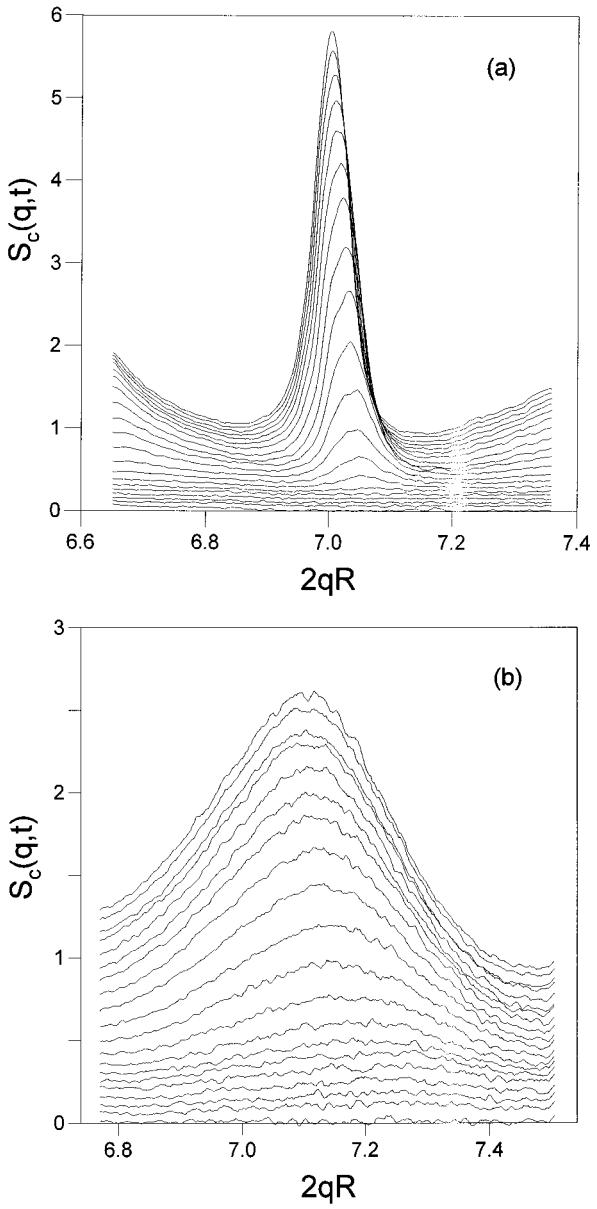

FIG. 4. As in Fig. 3, but now showing crystal structure factors, in arbitrary units, obtained from the total structure factors after subtraction of scattering by fluid. See text for further details.

increase. For the sample with concentration $\phi=0.548$, close to the melting value, however, there is an interval where the crystal dimension increases as the square root in time (see Fig. 10). The increase in L with time, seen for suspension concentrations up to about ϕ_m contrasts the behavior at higher concentrations where, during the interval over which $X(\tau)$ shows its sharpest rate of increase, the crystal size remains virtually constant.

The crystal number densities $N_c(\tau)$ [calculated from Eq. (6)] are shown as functions of time in Fig. 11. These results reflect more explicitly the change, apparent from the behavior of $L(\tau)$ and $X(\tau)$, in the crystallization mechanism that occurs around the melting concentration. Both the maximum rate of addition of crystals and the maximum number of crystals increase sharply, by more than two orders of magnitude, as the suspension concentration traverses the melting

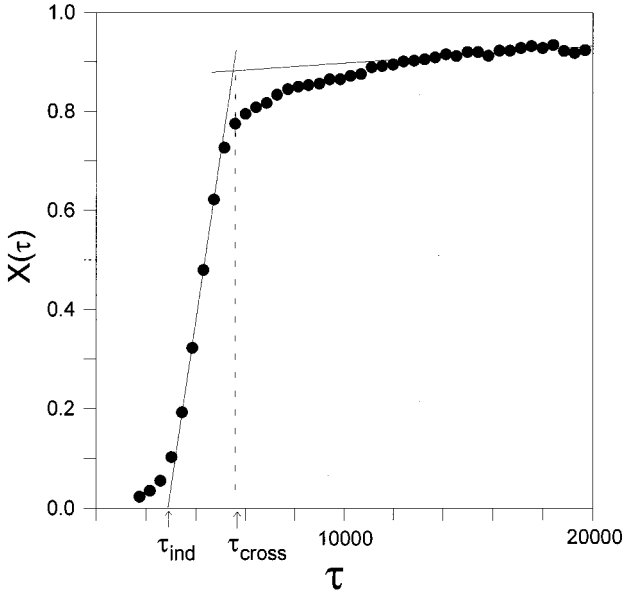

FIG. 5. Fraction of crystal vs time for $\phi=0.548$. Time is reduced with respect to the Brownian time, as discussed in the text. Also shown are the induction and crossover times $\tau_{\rm ind}$ and $\tau_{\rm cross}$, respectively.

value. Power-law exponents ν, corresponding to the steepest sections of $\log_{10}[N_c(\tau)]$ versus $\log_{10}[\tau]$, are shown in Fig. 8. The maximum nucleation rate densities $R_{\rm max}=(dN_c(\tau)/d\tau)_{\rm max}$ and the maximum crystal number densities, $N_{\rm max}$, are shown as functions of the suspension concentration in Fig. 12. Average nucleation rate densities $R_{\rm av}$, calculated from the time to reach $N_{\rm max}$, are also included in this figure.

From the position of the Bragg peak we calculate, using Eq. (7), the time dependence of the average volume fraction

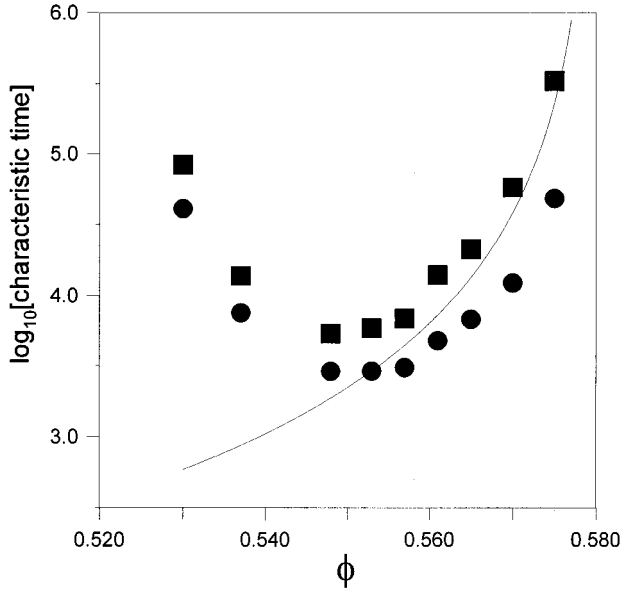

FIG. 6. Logarithm of characteristic times $\tau_{\rm ind}$ (●) and $\tau_{\rm cross}$ (■) vs volume fraction. The solid line shows the (dimensionless) time $\tau_I=D^{-1}$, where $D=(1-\phi/\phi_g)^{2.6}$ represents a fit to the measured [29] long-time single-particle diffusion coefficients. See text for details.

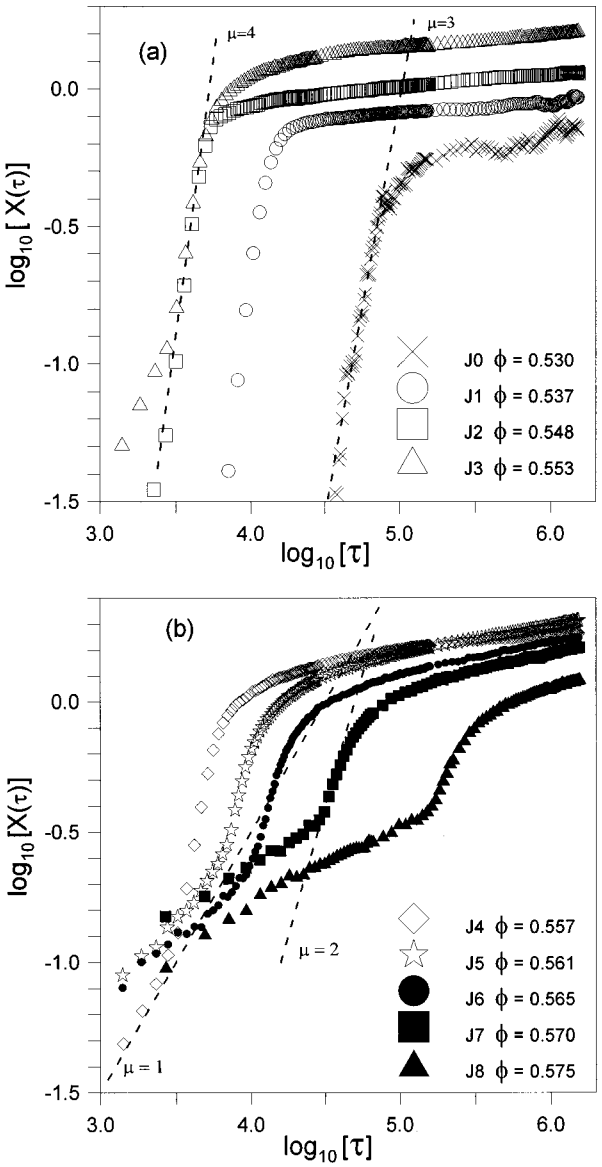

FIG. 7. Logarithm of the fraction of crystal vs the logarithm of reduced time. Suspension volume fractions are indicated. Power laws $X \sim \tau^{\mu}$ are drawn by dashed lines for exponents μ indicated.

$\phi_c(\tau)$ of the crystal phase. This is shown for the different suspension concentrations in Fig. 13. Then, with the aid of the equations of state for the hard-sphere fluid and crystal, we obtain the volume fraction $\phi_l(\tau)$ shown in Fig. 14, of the fluid in mechanical equilibrium with the crystal. From Figs. 7, 13, and 14, one sees that conversion of fluid to crystal is accompanied by decreases in volume fractions of both crystal and fluid phases. The second estimate of the fraction of the sample occupied by crystal, $X^*(\tau)$ [Eq. (8)], is shown in Fig. 9.

The initial and final crystal volume fractions $\phi_c(0)$ and $\phi_c(t_f)$, and initial and final fluid volume fractions $\phi_l(0)$ and $\phi_l(t_f)$, obtained from Figs. 13 and 14, respectively, are listed in Table I. An indication that equilibrium has effectively been established at the termination of the measurements for the lowest suspension concentrations ($\phi < \phi_m$) is evident from the observation that the crystal volume fraction at the time $t = t_f$ is, within experimental uncertainties, equal to the

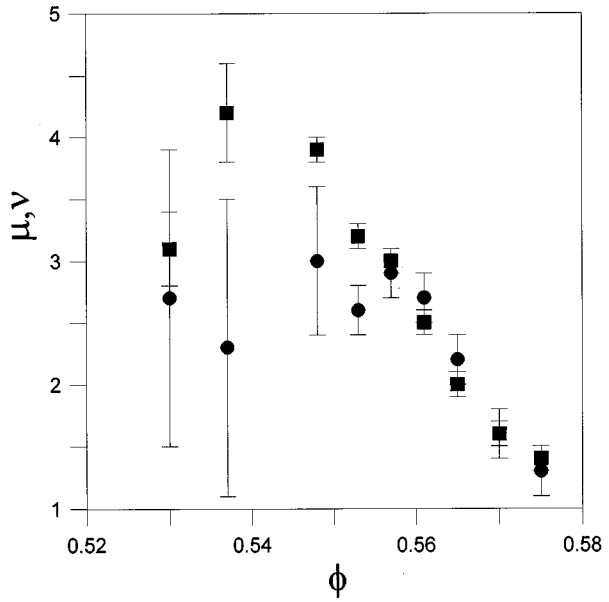

FIG. 8. Power-law exponents μ and ν vs volume fraction, for the fraction of crystal $X(t) \sim t^{\mu}$ (■) and number of crystals $N_c(t) \sim t^{\nu}$ (●).

melting concentration [i.e., $\phi_c(t_f) \approx \phi_m$].

Table II displays the times $\tau(X_{\max})$, $\tau(N_{\max})$, and $\tau(\dot{\phi}_{\max})$ where we find the maximum rate of crystallization, the maximum rate of addition of crystal, and the maximum rate of crystal lattice expansion, respectively. Due to experimental errors, mentioned above, any differences between these times are probably not significant for the lowest two suspension concentrations. However, for $\phi \geqslant 0.548$, errors in these times are down to about 3%, and the significance of the differences between them will be discussed below.

Finally, from the crystal number densities $N_c(\tau)$ (Fig. 11), and the concentration $\phi_l(\tau)$ (Fig. 14), of uncrystallized sus-

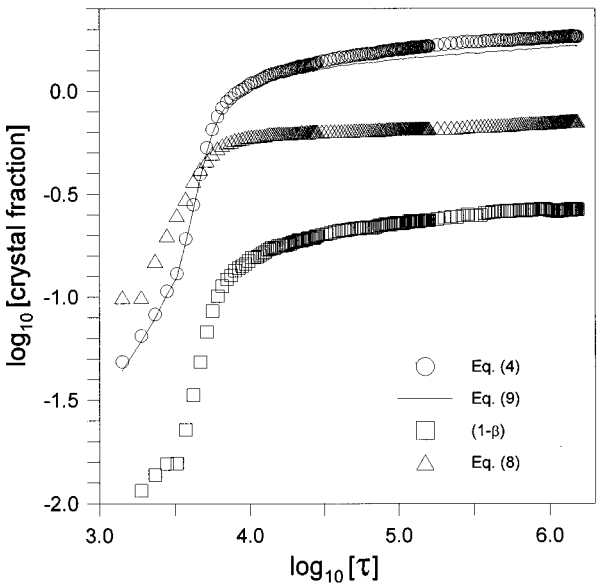

FIG. 9. Logarithm of the fraction of crystal, estimated by methods indicated, vs the logarithm of reduced time for $\phi = 0.557$. See text for details.

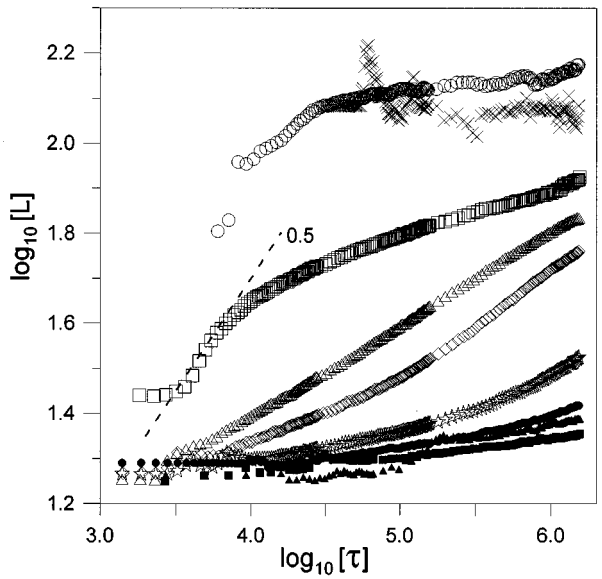

FIG. 10. Logarithm of the average linear crystal dimension (in particle diameters) vs the logarithm of reduced time. Suspension volume fractions are as indicated in Fig. 7. The dashed line indicates the power law $L \sim t^{(0.5)}$.

pension in mechanical equilibrium with the crystal, we eliminate τ to obtain $R_c(\phi_l)$. The latter quantity expresses the nucleation rate densities, shown in Fig. 15, in terms of the actual prevailing concentration of colloidal fluid. This expression of the nucleation rate is arguably more meaningful than maximum nucleation rate densities expressed as functions of the total suspension concentration (shown in Fig. 12). For $\phi \lesssim \phi_m$ the estimated total errors in $R_c(\phi_l)$, due to accumulation of experimental errors and possible systematic errors in reading ϕ_l from the equations of state, are too large to obtain meaningful results by this procedure.

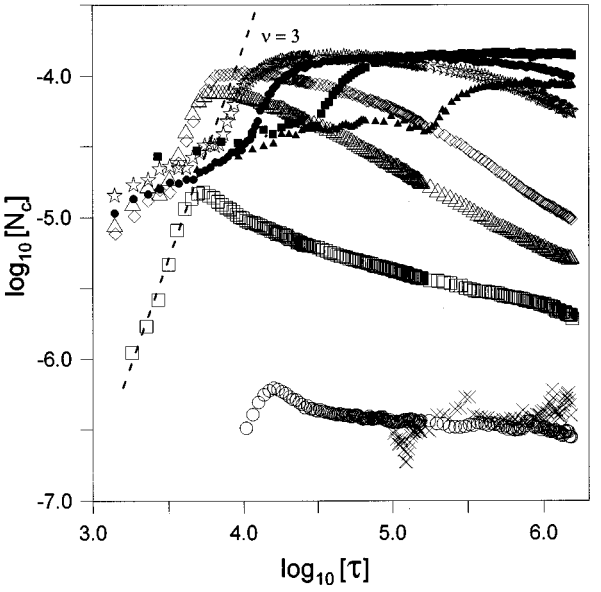

FIG. 11. Logarithm of the number density [in units of $(2R)^{-3}$] of average sized crystals vs the logarithm of reduced time. Suspension volume fractions are as indicated in Fig. 7. The dashed line is the power law $N_c \sim t^{\nu}$ for $\nu=3$.

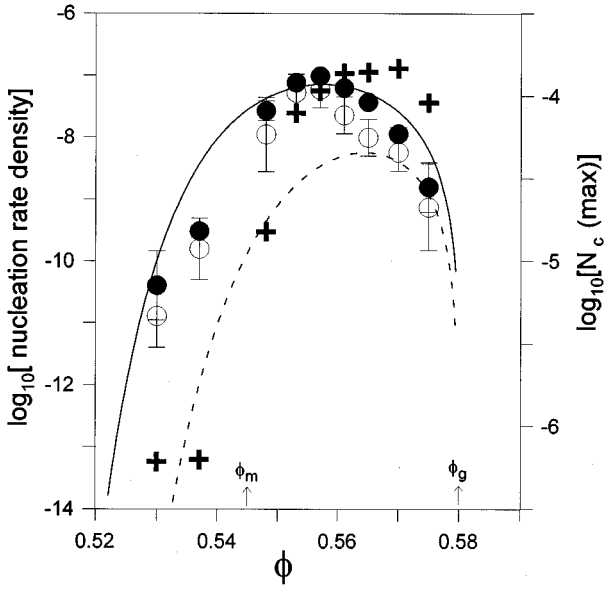

FIG. 12. Experimental maximum crystal number densities N_c(max), (+), maximum nucleation rate densities $R_{\max}$ (●), and average nucleation rate densities $R_{\rm av}$ (○). Also shown are nucleation rate densities calculated from Eq. (10) for $\gamma=0.65$ (dashed line) and $\gamma=0.50$ (solid line). Nucleation rate densities are in dimensionless form, in units of $D_0(2R)^{-5}$.

IV. DISCUSSION

A. Intensities and widths of Bragg peaks

We begin with a discussion of the features inferred from the intensities and widths of the Bragg peaks. The broad features of the crystallization processes that occur in these hard-sphere suspensions are displayed in Fig. 7. The induction and crossover times ($\tau_{\rm ind}$ and $\tau_{\rm cross}$ shown in Fig. 6), which may be interpreted, respectively, as the time at which nucleation commences and the time for the completion of

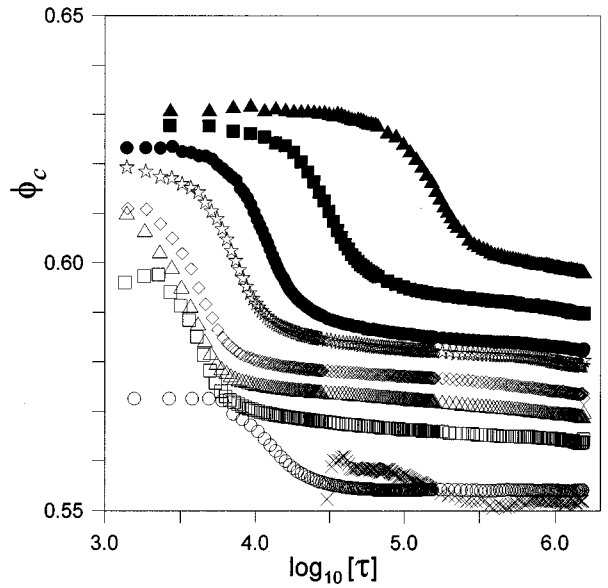

FIG. 13. Volume fraction of the crystal phase, $\phi_c(\tau)$, vs logarithm of the reduced time. Suspension concentrations are as indicated in Fig. 7.

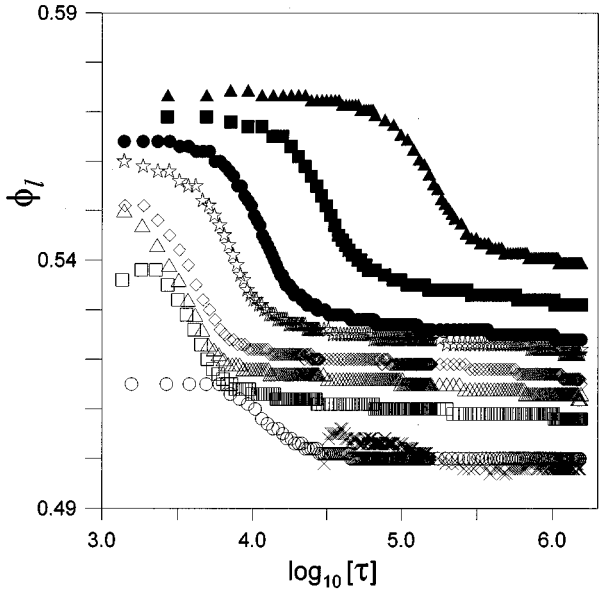

FIG. 14. Volume fraction of the fluid phase, $\phi_l(\tau)$, vs logarithm of the reduced time. Suspension concentrations are as indicated in Fig. 7.

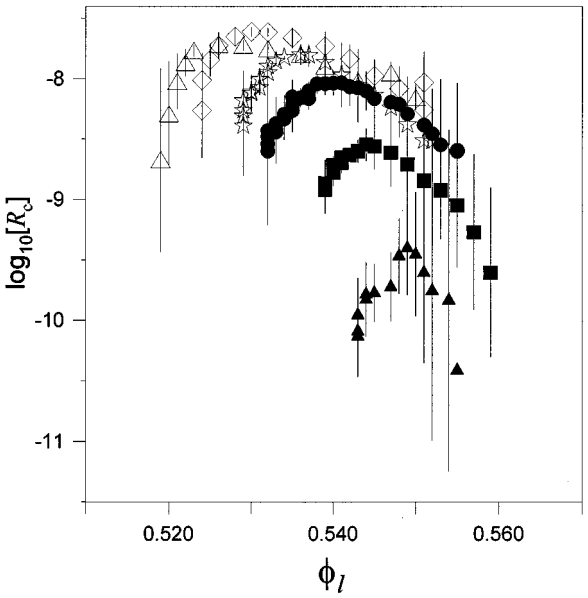

FIG. 15. Nucleation rate density $R_c(\phi_l)$ vs actual volume fraction of the fluid phase. Suspension concentrations as indicated in Fig. 7. Vertical lines indicate error estimates.

crystallization, quantify previous observations [28] that the crystallization rate varies nonmonotonically with the suspension concentration, between freezing and the glass transition, with a maximum rate occurring around the melting concentration ϕ_m. Note also that as the glass transition concentration ϕ_g is approached, $\tau_{\rm ind}$ and $\tau_{\rm cross}$ scale approximately with the inverse of the long-time single-particle diffusion coefficient [29]. For the purposes of the following discussion we define the (concentration) quench depth by the quantity $\Delta=(\phi-\phi_f)/(\phi_m-\phi_f)$, so that ϕ_m is the concentration that delineates shallow ($\Delta<1$) from deep ($\Delta>1$) quenches.

In Figs. 7 and 11 three stages of fluid to crystal conversion $X(\tau)$, and crystal addition $N_c(\tau)$, can be identified: (i) an initial relaxation stage which becomes slower with increasing suspension concentration; (ii) a fast stage of conversion, associated with nucleation and growth, that crosses over to (iii) a stage of much slower conversion that might be identified with coarsening. We discuss each of these stages in turn.

(i) As the suspension concentration is raised an increasingly prominent slow stage of conversion (Fig. 7) and crystal addition (Fig. 11) precedes the stage of rapid nucleation and growth. We attribute this slow stage to the relaxation of residual shear-aligned structures formed during tumbling of the samples. It seems plausible that, with increasing suspension concentration, dissipation of any strongly asymmetric, and therefore thermodynamically unstable, structures becomes slower and competes increasingly with the process of homogeneous nucleation. In colloidal glass ($\phi>\phi_g$) these shear-aligned structures appear to remain partly intact, and seed the growth of quite large and irregularly shaped crystals [23].

(ii) From Fig. 7 one sees that, at least over a limited interval, the stage of most rapid crystallization can be de-

TABLE II. The first column shows the sample concentrations ϕ; $\tau(\dot{X}_{\rm max})$, $\tau(\dot{N}_{\rm max})$, and $\tau(\dot{\phi}_{\rm max})$ are, respectively the times corresponding to the maximum rate of crystallization $(dX/d\tau)_{\rm max}$, the maximum rate of nucleation $(dN_c/d\tau)_{\rm max}$, and the maximum rate of reduction $-(d\phi_c/d\tau)_{\rm max}$ of the concentration of the crystal phase. (Errors in the stated times are about 3% for all except the lowest two concentrations where they are about 20%). The fifth column lists the time differences $\delta\tau=\tau(\dot{X}_{\rm max})-\tau(\dot{\phi}_{\rm max})$, and the last column lists the times $\tau_I=D^{-1}$ required for a particle to diffuse a distance equal to its radius; the diffusion coefficient is given by the expression $D=(1-\phi/\phi_g)^{2.6}$, which fits the measured long-time single-particle diffusion coefficients. The times shown here are expressed in units of the free-particle characteristic Brownian time (see Sec. IV A for further details).

ϕ	$\tau(\dot{X}_{\rm max})$	$\tau(\dot{N}_{\rm max})$	$\tau(\dot{\phi}_{\rm max})$	$\delta\tau$	τ_I
0.530	6.9×10^4		4.1×10^4		5.8×10^2
0.537	1.1×10^4	1.0×10^4	1.1×10^4		8.7×10^2
0.548	4.5×10^3	3.5×10^3	4.0×10^3	4.6×10^2	1.8×10^3
0.553	4.5×10^3	4.3×10^3	3.2×10^3	1.4×10^3	2.9×10^3
0.557	5.1×10^3	4.9×10^3	4.1×10^3	9.4×10^2	4.4×10^3
0.561	8.1×10^3	7.9×10^3	6.4×10^3	1.8×10^3	7.2×10^3
0.565	1.3×10^4	1.3×10^4	9.6×10^3	3.7×10^3	1.3×10^4
0.570	3.7×10^4	3.7×10^4	3.1×10^4	6.5×10^3	3.8×10^4
0.575	2.1×10^5		1.6×10^5	5.3×10^4	2.3×10^5

scribed by a power law, i.e., $X(\tau)\sim\tau^{\mu}$. The growth exponents μ shown in Fig. 8 range from about 4, at the lowest concentrations studied, to around 2 as the glass transition is approached.

For shallow quenches ($\phi<\phi_m$ or $\Delta<1$) [Fig. 7(a)] the fast increase in $X(\tau)$ is accompanied by a significant increase in the average linear crystal size, $L(\tau)$ (Fig. 10). As discussed in Sec. III, experimental noise does not allow us to specify the power-law growth exponents for $L(\tau)$ at the two lowest concentrations, $\phi=0.530$ and 0.537.

Since $X(\tau)=L^3(\tau)N_c(\tau)\sim\tau^{\mu}$ and $\mu\approx3$ for $\phi=0.530$ and $\mu\approx4$ for $\phi=0.537$, one obtains, by assuming constant nucleation rates, crystal growth exponents of about 0.7 and 1.0, respectively. These exponents agree with those obtained from small angle scattering on suspensions of the same particles [30]. However, the assumption of a constant nucleation rate cannot be justified on the basis of our data, and the possibility of accelerated nucleation along with more retarded crystal growth laws cannot be precluded for the lowest two suspension concentrations studied here. Indeed, at the slightly higher concentration, $\phi=0.548$ (sample $J2$), where the data permits better resolution of the peak width at early times, growth is slower and sublinear [$L(\tau)\sim\tau^{1/2}$] (Fig. 10) and the accompanying nucleation (Fig. 11) is clearly accelerated. Whether this sublinear growth applies to an isolated crystal can obviously not be discerned by means of these or, for that matter, small angle, scattering experiments.

At still higher concentrations ($\phi\gtrsim0.55$), or deeper quenches ($\Delta>1$), the observed crystallization is qualitatively different. The smallest crystal size detected, $L\approx20$, remains virtually constant over the time interval where $X(\tau)$ [Fig. 7(b)] shows its strongest rate of increase, suggesting that crystallization is dominated by nucleation. Moreover, as indicated by the fact that the power-law exponents exceed unity, nucleation is accelerated: $X(\tau)\sim N_c(\tau)\sim\tau^{\nu}$, with $\nu>1$ (see Figs. 8 and 11). The approximate agreement between the maximum and average nucleation rate densities $R_{\max}$ and $R_{\rm av}$ at the higher suspension concentrations (Fig. 12) suggests that crystallization proceeds by the appearance of crystals in a burst. This sudden appearance of large numbers of nuclei, separated by regions of fluid that extend only about 20 particle diameters, seems to be responsible for suppressing significant crystal growth.

(iii) At the longest times the combination of the slow increase in the average linear crystal dimension $L(\tau)$ (Fig. 10), and slow decrease in the number of crystals $N_c(\tau)$ (Fig. 11), indicates coarsening of large crystals at the expense of smaller ones. However, the intensity of the Bragg reflection continues to increase, albeit at a much slower rate, to the end of the measurement. In addition, we find that the power-law growth exponents associated with the increase in crystal size at long times (Fig. 10) range from about 0.005 to about 0.2. These values are smaller than 0.5, predicted for the classical coarsening process of crystals in contact [31]. These features suggest the existence of processes other that coarsening. Two explanations are offered here.

First, due to the polydispersity, which is about 5% for the particles used in these experiments, some compositional change may occur as the particles from the middle of the particle size distribution are preferentially accommodated into nuclei and growing crystals. Indeed recent Monte Carlo simulations by Bolhuis and Kofke [32], who computed the coexisting solid-fluid phase boundaries for hard spheres with continuous and symmetrical particle size distributions, showed that the solid phase has a lower polydispersity than the fluid. For a system with an average polydispersity of 5% the difference in polydispersity of coexisting fluid and solid phases was found to be about 1%. Although the fractionation required to attain this small difference in composition may pose a negligible kinetic impediment during initial nucleation and growth, ensuing growth may be strongly hindered due to the need for increasingly significant particle rearrangements as an increasing fraction of dissimilar particles becomes trapped in the regions between the crystals. This slow ongoing growth will contribute to the intensity of the Bragg peak, but it may also delay the onset of coarsening of crystals in contact and obstruct its progress. While the largest power-law exponents extracted here from the long-time behavior of the average crystal size are smaller than predicted by the classical coarsening model, the increasing slopes of $\log_{10}[L(\tau)]$ versus $\log_{10}[\tau]$ seen at long times (in Fig. 10) also suggest the possibility that the classical coarsening process has not been attained during the period of observation.

Second, recent measurements imply [33] that the extent of random stacking slowly decreases when these colloidal crystals are left undisturbed for long periods. The gradual reduction in stacking faults as the stress on the crystals is relaxed (see Fig. 13) will increase the fraction of close-packed planes and, as seen in Fig. 7, gradually increase the intensity of the corresponding Bragg reflection. Our detector window was too narrow to observe the other signatures associated with random stacking effects [24,33].

In Fig. 7(a) one sees that the fraction of crystal, $X(t_f)$, present at the termination of the measurements increases with increasing suspension concentration. This increase in $X(t_f)$ is consistent with the increasing equilibrium fraction $[(\phi-\phi_f)/(\phi_m-\phi_f)]$ of crystal expected for samples with concentrations ($\phi=0.530$ and 0.537) between the freezing and melting values. Recall that $X(\tau)$ has been normalized so that $X(t_f)=1$ for $\phi=0.545$. However, as the suspension concentration is increased [Fig. 7(b)], $X(t_f)$ continues to increase to a maximum value, given by $\log_{10}(X(t_f))\approx0.3$ at $\phi=0.561$. Since we have already concluded that crystallization is dominated by nucleation at the higher concentrations, a corollary to the suggestion of the preceding paragraph is that fewer stacking faults are formed during nucleation than during growth. Current work is aimed at addressing this issue. Beyond the concentration $\phi=0.561$, $\log_{10}(X(t_f))$, decreases, presumably due to the rapidly slowing particle diffusion as the glass transition is approached [22,29].

B. Peak positions

In this section we discuss the behavior determined from the position of the Bragg peak. Figures 13 and 14 indicate that in all cases the volume fractions of the crystal phase and the fluid phase decrease monotonically with time. Since the total volume of suspension is fixed, a decrease in the volume fraction of the fluid is expected to accompany the formation of a solid phase that is more densely packed than the fluid. The reduction in ϕ_l produces a decrease in the (normal) stress on the crystals and allows them to relax. From these

results and Table I, one observes that for samples whose total concentrations (ϕ=0.530 and 0.537) are below melting, $\phi_l(t_f)$ and $\phi_c(t_f)$ coincide, within experimental error, with the freezing and melting concentrations ϕ_f(=0.494) and ϕ_m(=0.545), respectively, of the hard-sphere system. Thus, at the termination of the measurement (t_f=20 h), these suspensions have phase separated into crystal and fluid in equilibrium. For $\phi>\phi_m$ one expects, at equilibrium, a crystal phase with volume fraction equal to that of the sample. Since t_f is the same for all experiments, the increasing difference $\phi_c(t_f)-\phi$ between the volume fraction of the crystal phase at $t=t_f$ and the (total) volume fraction of the sample (i.e., the difference between ϕ and $\phi_c(t_f)$ in Table I) indicates a progressively slower approach to equilibrium as the suspension concentration is increased.

One also sees, from Table I, that the volume fractions of the first identified crystals are significantly higher than the total volume fraction of the suspension. In fact, the initial crystals have a volume fraction greater than the volume fraction at melting [$\phi_c(0)>\phi_m$], even when the (average) suspension volume fraction is less than the melting value. By comparing the values for ϕ and $\phi_l(0)$ (Table I), one notices that, for shallow quenches, the volume fraction of the fluid in mechanical equilibrium with the crystal is significantly less than that of the suspension, i.e., $\phi_l(0)<\phi$. Bearing in mind that when the Bragg peak can be first identified with confidence only a few percent of the suspension has actually crystallized, the picture that emerges is one where the crystals are encapsulated by a region of fluid of lower concentration than the average suspension concentration. As discussed recently by Ackerson and Schätzel [11,12], a depletion zone develops during the growth of crystals in the coexistence region for systems, such as hard spheres, where there is a significant concentration difference between (equilibrium) crystal and fluid phases.

Note also from Table II that, for ϕ=0.548, $\tau(\dot{N}_{\max})<\tau(\dot{X}_{\max})$ and $\tau(\dot{X}_{\max})\approx\tau(\dot{\phi}_{\max})$. It is evident, therefore, that nucleation precedes crystal growth, but that lattice expansion occurs at the same time as crystal growth. (Experimental uncertainties prevent quantitative comment for the lowest two concentrations).

For shallow quenches our observations, along with the small angle scattering studies in Refs. [11] and [30], suggest that solidification proceeds by the formation of isolated nuclei and crystal growth. The results suggest further that, to varying degrees, growth is limited by diffusion of particles to the crystal-fluid interface, and that growth is the dominant mechanism by which fluid is converted to crystal.

Continuing the discussion of Figs. 13 and 14 and Table II for deep quenches, one sees that, for $\phi>0.55$, $\phi_l(0)\approx\phi$, i.e., the volume fraction of the fluid in pressure balance with the crystal phase is almost identical to the (total) volume fraction of the suspension. Thus, if the colloidal crystal and fluid phases obey the equations of state predicted for the hard-sphere system, a premise supported by the equilibrium phase behavior observed for these suspensions (see Sec. II A, and Refs. [6] and [16]), these results indicate that the first crystals observed are effectively in mechanical equilibrium with the fluid. However, when comparing (in Fig. 9) the estimates of the fraction of crystal, $X(\tau)$, obtained directly from the Bragg peak intensity [Eq. (4)] and $X^*(\tau)$, based on the assumption of mechanical equilibrium between fluid and crystal phases [Eq. (8)], one notices that $X(\tau)$ lags $X^*(\tau)$ slightly.

From Table II one sees that for deep quenches, since $\tau(\dot{X}_{\max})\approx\tau(\dot{N}_{\max})$, crystallization and nucleation occur together. However, $\tau(\dot{\phi}_{\max})<\tau(\dot{X}_{\max})$, i.e., nucleation lags lattice expansion. A possible picture suggested by these observations is that the concentration gradients, produced in the colloidal fluid in the wake of nucleation, relax prior to further nucleation. The time intervals (Table II) $\delta\tau=\tau(\dot{X}_{\max})-\tau(\dot{\phi}_{\max})$ are significantly smaller than the times τ_I required for a particle to diffuse a distance equal to its radius. The times $\delta\tau$ may be sufficient, however, for the relaxation of concentration fluctuations of wavelength comparable to the estimated average surface to surface distance, about 20 particle diameters, between the nuclei. We note that for suspensions of hard-sphere particles, the collective diffusion coefficient characterizing relaxation of concentration fluctuations on this scale is almost independent of the concentration [34].

The nucleation rate densities are shown in Fig. 15 for each suspension concentration ($\phi>0.55$) as functions of the prevailing (average) fluid concentration. A reasonable coincidence of the nucleation rates is obtained for colloidal fluid concentrations, ϕ_l, from about 0.535 to about 0.555, for the four samples $J3-J6$. Thus, during the initial stages of nucleation, pressure balance between crystal and fluid appears to be maintained, and the nucleation rate is independent of the initial suspension concentration. At the highest two suspension concentrations initial nucleation is more strongly suppressed than at lower concentrations by relaxation of the sheared fluid. As nucleation proceeds, the time lags between the nucleation and relaxation of crystal and fluid concentrations, discussed in the preceding paragraph, translate (via Fig. 14) into the diverging nucleation rates, seen in Fig. 15, when the fluid concentration falls below about 0.535.

C. Effects of polydispersity

As mentioned in Sec. IV A, Bolhuis and Kofke [32] recently explored the freezing-melting transition of assemblies of hard spheres with continuous particle size distributions PSD's by means of Monte Carlo computer simulation. They found that polydispersity alters the volume fractions of the coexisting solid and fluid phases; for a system with an average polydispersity of 5% the freezing and melting volume fractions increase, respectively, from 0.494 and 0.545, the values for the one-component hard-sphere system, to about 0.502 and 0.550 (as read from Fig. 3 of Ref. [32]). Therefore, one could argue that in order to allow for the effects of the 5% polydispersity, estimated for the suspensions used here, the stated effective hard-sphere volume fractions should be multiplied by the factor 0.502/0.494. However, to facilitate comparison with previous studies of the particle dynamics and the glass transition [22], which were performed on the same suspensions as the crystallization studies reported in this paper, we refrain from applying this multiplication here.

In another recent experimental study [35] the particle dynamics and crystallization kinetics were compared for suspensions of hard-sphere PMMA particles with polydispersi-

ties of 6% and 11%. However, the broader PSD was negatively skewed rather than symmetrical, as used in the computer simulations [32]. No appreciable difference in the equilibrium phase behavior was found between the two suspensions and, when the volume fractions were scaled by the one-component hard-sphere freezing volume fraction, as outlined in Sec. II A, no significant differences in the particle dynamics nor the location of the glass transition were observed. The only significant difference in the observed behavior of the two suspensions was that crystallization in the more polydisperse system was about ten times slower. This reduction in the crystallization rate was rationalized in terms of a fractionation process in which the smaller particles are ejected from the nucleating and growing crystals [35].

The experiments in this paper and those on Ref. [35], along with density functional theory [36] and computer simulation [37], which predict partial demixing on solidification of a binary mixture of hard spheres when the difference in radii exceeds about 6%, and complete demixing when the difference is 15% or more, suggest the following scenario for the crystallization process of polydisperse suspensions. When the polydispersity is small, say less than about 5%, the fraction of particles that cannot be incorporated into the crystal phase is small and, as conjectured in Sec. IV A, only growth at late stages, when the final complement of crystal is close to being attained, and coarsening are likely to be impeded by the need to eject particles from the extremities of the PSD. However, in systems with significantly larger polydispersity there will be an increasing requirement for fortuitous composition fluctuations to occur in concert with concentration fluctuations in order to form nuclei and effect growth. The symmetry of the PSD is also likely to play a significant role. It is not difficult to appreciate that a polydisperse system in which the PSD is negatively skewed is more favorably disposed to crystallization, in kinetic terms, than those with an equivalent but positively skewed PSD. The issue of polydispersity is interesting and important, and we are presently engaged in a systematic study of the influence of polydispersity on the particle dynamics and crystallization kinetics.

D. Classical nucleation theory

The classical theory of nucleation [4,5], recently reformulated for hard spheres [38,39], gives the following result for the nucleation rate density:

$$R_{\mathrm{class}}=A\phi^{5/3}D\ \exp\left[-\frac{4\pi^3\gamma^3}{27\phi^2\Delta\mu^2}\right],$$

where γ [in units of $kT/(2R)^2$] is the surface tension of the fluid-crystal interface, $\Delta\mu$ (in units of kT) is the difference in the chemical potential between the crystal and fluid phases, A is a dimensionless factor, and D is the particle diffusivity relative to the free-particle diffusion constant, D_0. In evaluating R_{class} we calculate $\Delta\mu$ from the equations of state of the hard-sphere crystal [26] and metastable fluid [27]. For the dimensionless diffusivity we use the expression $D=(1-\phi/\phi_g)^{2.6}$ which fits to the long-time single-particle diffusion coefficient measured on metastable fluids of these particles [29]. The constant A and the surface tension are treated as free parameters.

R_{class} is shown in Fig. 12 for two values of γ with $A=0.01$. Since R_{class} follows the data for values of γ that fall in the range of current theoretical and computational estimates for the surface tension of the fluid-crystal interface of hard spheres [40], it seems that nucleation in hard-sphere suspensions can be described by classical nucleation theory. It should be mentioned, however, that the theoretical estimates of γ apply to planar interfaces separating fluid and crystal in equilibrium. The extent to which these estimates apply to the curved interfaces and the nonequilibrium conditions that prevail during the crystallization process is not clear.

With the aid of Fig. 12 it is not difficult to appreciate a possible mechanism for the accelerated nucleation seen in Fig. 11. When the colloidal fluid is quenched to a concentration to the right of the maximum in R_{max} versus ϕ, the nucleation of crystals more compact than the fluid results in a reduction in the concentration of the remaining fluid (Fig. 14) in which, according to Fig. 12, the nucleation rate is greater than in the original fluid. Thus nucleation is a positive feedback process for $\phi\gtrsim\phi_m$.

Caution must be exercised, however, in interpreting the above as confirmation of classical nucleation theory, certainly at the higher suspension concentrations. First, R_{class} is very sensitive to the details of the equations of state and, as Fig. 12 illustrates, to the value of γ. Second, if the nucleation could be described by the formation of isolated nuclei, one would expect to find the nucleation rate density to be a unique function of the concentration of the fluid, ϕ_l, and independent of the total suspension concentration, ϕ. For deep quenches the results of Fig. 15 show this not to be the case in general. Rather than independent nucleation events, the time lags between lattice expansion and nucleation and the accelerated nucleation suggest that nucleation events observed here are strongly coupled.

E. Small angle light scattering

Small angle light scattering (SALS) has also been used to study the crystallization kinetics of suspensions of PHSA-stabilized PMMA particles [11,30]. In these latter studies tetralin instead of CS_2 was mixed with decalin to achieve refractive index matching of particles and suspending liquid. However, previous work with these suspensions [16] indicates that this difference in solvent has no effect other than a change in the solvent viscosity. In SALS the amount of crystal and the crystal size are obtained from the maximum intensity I_m and the position $q_{1/2}$ of the low angle peak [11]. This method gives the strongest signal at low suspension concentrations ($\phi\lesssim\phi_m$) where scattering arises from large isolated crystals but then the signal deteriorates for concentrations above the melting value. SALS therefore compliments the Bragg angle scattering employed here, which is clearly most reliable at higher concentrations ($\phi\gtrsim\phi_m$) where scattering emanates from large numbers of randomly oriented crystals.

In the concentration range, from about 0.53 to about 0.55, where the two techniques overlap, significant similarities can be inferred from the respective results. In SALS, nucleation

and growth are identified with an initial sharp increase in I_m. This intensity increase is accompanied by a significant decrease in $q_{1/2}$ for $\phi \leqslant 0.545$, but it remains almost constant for higher concentrations. The crystallization mechanism indicated by these observations is crystal growth that is generally sublinear (diffusion controlled), accompanied by a constant rate of nucleation below the melting concentration, and accelerated nucleation with comparatively suppressed crystal growth above melting. Crossover from nucleation and growth to coarsening can be identified at times, τ_{cross} that are in agreement with those obtained here.

An important difference between the two techniques is that Bragg scattering is sensitive only to those regions, with average linear dimension L, of an imperfect crystal or polycrystal that satisfy the Bragg condition, and the scattered intensity is proportional to L^3. In SALS the scattered intensity is proportional to the square of the volume of the whole polycrystal. For these reasons the behavior observed in the coarsening regime, at long times, differs for the two approaches. Where the Bragg peak intensity $X(\tau)$ increases monotonically (see Fig. 7), I_m obtained in SALS show significant dips for $\tau > \tau_{\text{cross}}$ before increasing in a manner that is consistent with coarsening. These intensity dips have been attributed to the breakup of crystals along grain and facet boundaries under the action of gravitational stresses.

F. Computer simulation

Computer simulation provides a view on microscopic length and time scales that is often inaccessible experimentally and, since the first discovery of a nucleation event by Mandell, McTague, and Rahman [41], numerous molecular dynamics simulations have explored the process of homogeneous nucleation in undercooled liquids of simple atoms [42]. In more recent simulations [43,44] it has been possible to delineate the formation of a critical nucleus from the onset and completion of rapid growth. For shallow quenches the nuclei are compact, and the time lag between nucleation and growth, signaled by the release of latent heat, decreases with quench depth. These features appear to be in accord with classical theory. For deep quenches, however, the critical nuclei have a ramified, or some other thermodynamically unstable, structure [42]. The times to nucleation and completion of growth are independent of the quench depth, but the time interval from nucleation to the commencement of growth decreases with quench depth [42]. In addition, the single-particle diffusion coefficient shows only a weak temperature dependence. These findings for deep quenches cannot be reconciled in terms of classical theory, and the explanation given for the appearance of unstable critical nuclei and the increasing time lags is that nucleation is influenced by an underlying spinodal [43,45].

It may be tempting to relate the departures from classical nucleation theory, observed for deep quenches, in computer simulations with those in these hard-sphere suspensions. However, there are important differences. First, while the occurrence of strongly coupled nucleation events, observed here for $\Delta > 1$, may be symptomatic of spinodal behavior, τ_{ind} and τ_{cross} (Fig. 6) scale with the inverse of the diffusion coefficient, which is a strong function of the quench depth. This suggests that the slowing down in nucleation, observed in the present work, is associated with the slowing of diffusion as the glass transition is approached rather than critical slowing. Second, we cannot identify a time lag between nucleation and growth because, for deep quenches we find growth suppressed by very high nucleation rate densities. Third, the number of particles in the first identifiable crystals is of order 1000, whereas the critical nuclei seen in the simulations are composed of tens of atoms.

Finally, we should point out that we associate the first identifiable feature that discerns itself from the fluid structure with the interlayer reflection from close-packed planes. In this sense we essentially preclude potential identification of the ramified structures [42], and possibly other thermodynamically unstable precursors [46], found in computer simulation studies. Current experimental work that explores crystallization kinetics over a much broader spatial window than that used in the experiments reported here has so far failed to give any tangible evidence for the existence, although possibly transient, of structures other than close packed.

V. CONCLUSIONS

Crystals in suspensions of particles with hard-sphere-like interactions consist of randomly stacked close-packed layers. Between freezing and the glass transition, crystallization proceeds by homogeneous nucleation. From the moments of the interlayer reflection we calculate the amount of crystal, the average linear crystal size, the number of crystals, and the average volume fraction of the crystal phase as functions of time. In contrast to previous studies, crystal nucleation and growth rates are obtained free from any assumptions concerning their time dependencies.

For shallow quenches we find that crystallization proceeds by nucleation and growth. Moreover, a slight time lag between nucleation and fluid to crystal conversion points to the classical picture of sequential nucleation and growth. Our findings for shallow quenches are compatible with those of SALS studies on suspensions of particles similar to those used here.

For deep quenches we find several interesting features. First, crystal growth is suppressed by high nucleation rates. In addition, we observe nucleation rates that are accelerated rather than constant as is generally assumed. Second, the concentrations of the fluid and crystal phases decrease monotonically during the crystallization process. Third, the first identifiable crystals are in mechanical equilibrium with the fluid, and strongly compressed by it. Relaxation of the crystal lattice slightly precedes subsequent nucleation; we speculate that continued nucleation requires relaxation of concentration fluctuations induced in the fluid by prior nucleation events.

ACKNOWLEDGMENTS

This work was supported by the Australian Research Council. We thank Phil Francis for his technical assistance, and Sylvia Underwood for the preparation of the suspensions. We also acknowledge many valuable discussions with Bruce Ackerson, Peter Harrowell, Stuart Henderson, Sylvia Underwood, and Heiner Versmold.

[1] P. N. Pusey, in *Liquids, Freezing and the Glass Transition*, edited by J. P. Hansen, D. Levesque, and J. Zinn-Justin (North-Holland, Amsterdam, 1991), p. 763.
[2] W. van Megen and S. M. Underwood, Langmuir **6**, 35 (1990).
[3] D. J. W. Aastuen, N. A. Clark, L. K. Cotter, and B. J. Ackerson, Phys. Rev. Lett. **57**, 1733 (1986).
[4] K. F. Kelton, in *Solid State Physics*, edited by H. Ehrenreich and O. Turnbull (Academic, New York, 1991), Vol. 45, p. 75; *Ceramic Transactions, Nucleation and Crystallization in Liquids and Glasses*, edited by M. C. Weinberg (American Ceramic Society, Westerville, Ohio, 1993).
[5] J. Frenkel, *Kinetic Theory of Liquids* (Oxford University Press, Oxford, 1946).
[6] P. N. Pusey and W. van Megen, Nature (London) **320**, 340 (1986).
[7] H. N. W. Lekkerkerker, P. Buining, J. Buitenhuis, G. J. Vroege, and A. Stroobants, in *Observation and Simulation of Phase Transitions in Complex Fluids*, edited by M. Baus *et al.* (Kluwer, Amsterdam, 1995).
[8] P. Bartlett and W. van Megen, in *Granular Matter, an Interdisciplanary Approach*, edited by A. Mehta (Springer-Verlag, New York, 1994).
[9] W. van Megen, Transport Theory Stat. Phys. **24**, 1017 (1995).
[10] K. Schätzel, in *Ordering and Phase Transitions in Charged Colloids*, edited by A. K. Arora and B. V. R. Tata (VHC, New York, 1996).
[11] K. Schätzel and B. J. Ackerson, Phys. Rev. E **48**, 3766 (1993).
[12] B. J. Ackerson and K. Schätzel, Phys. Rev. E **52**, 6448 (1995).
[13] D. J. W. Aastuen, N. A. Clark, J. C. Swindal, and C. D. Munzy, Phase Trans. **21**, 139 (1990).
[14] J. K. G. Dhont, C. Smits, and H. N. W. Lekkerkerker, J. Colloid Interface Sci. **152**, 386 (1992).
[15] J. L. Harland, S. I. Henderson, S. M. Underwood, and W. van Megen, Phys. Rev. Lett. **75**, 3572 (1995).
[16] S. M. Underwood, J. R. Taylor, and W. van Megen, Langmuir **10**, 3550 (1994).
[17] P. N. Pusey and W. van Megen, J. Chem. Phys. **80**, 3513 (1984).
[18] W. van Megen and P. N. Pusey, Phys. Rev. A **43**, 5429 (1991).
[19] W. G. Hoover and F. H. Ree, J. Chem. Phys. **49**, 3609 (1968).
[20] S. E. Paulin and B. J. Ackerson, Phys. Rev. Lett. **64**, 2663 (1990).
[21] L. Verlet and J. J. Weis, Phys. Rev. A **5**, 939 (1972).
[22] W. van Megen and S. M. Underwood, Phys. Rev. E **49**, 4206 (1994).
[23] W. van Megen and S. M. Underwood, Nature (London) **362**, 616 (1993).
[24] P. N. Pusey, W. van Megen, P. Bartlett, B. J. Ackerson, J. G. Rarity, and S. M. Underwood, Phys. Rev. Lett. **63**, 2753 (1989).
[25] R. W. James, in *Optical Principles of Diffraction of X-Rays*, edited by L. Bragg (Cornell University Press, Ithaca, NY, 1965).
[26] N. F. Carnahan and K. E. Starling, J. Chem. Phys. **51**, 635 (1969).
[27] K. R. Hall, J. Chem. Phys. **57**, 2252 (1972).
[28] P. N. Pusey and W. van Megen, in *Physics of Complex and Supermolecular Fluids*, edited by S. A. Safran and N. A. Clark (Wiley-Interscience, New York, 1987).
[29] T. C. Mortensen and W. van Megen (unpublished).
[30] Y. He, B. J. Ackerson, W. van Megen, S. M. Underwood, and K. Schätzel, Phys. Rev. E **54**, 5286 (1996).
[31] I. Lifshitz and V. Solyozov, J. Phys. Chem. Solids **19**, 35 (1961).
[32] P. G. Bolhuis and D. A. Kofke, Phys. Rev. E **54**, 634 (1996).
[33] T.-T. Chui, Master's thesis, University of Edinburgh, 1994.
[34] M. M. Kops-Werkhoven and H. M. Fijnaut, J. Chem. Phys. **74**, 1618 (1981); W. van Megen, R. H. Ottewill, S. M. Owens, and P. N. Pusey, *ibid*. **82**, 508 (1985).
[35] S. I. Henderson, T. C. Mortensen, and W. van Megen, Physica A **233**, 109 (1996).
[36] A. R. Denton and N. A. Ashcroft, Phys. Rev. A **42**, 7312 (1990).
[37] W. G. T. Kranendonk and D. Frenkel, Mol. Phys. **72**, 679 (1991).
[38] W. B. Russel, Phase Trans. **21**, 127 (1990).
[39] J. S. van Duineveldt and H. N. W. Lekkerkerker, in *Science and Technology of Crystal Growth*, edited by J. P. van Erde and O. S. L. Bruinsma (Kluwer, Dordrecht, 1995).
[40] See, for example, A. Kirlidis and R. A. Brown, Phys. Rev. E **51**, 5832 (1995), and references cited therein.
[41] M. J. Mandell, J. P. McTague, and A. Rahman, J. Chem. Phys. **64**, 3699 (1976).
[42] R. D. Mountain, in *Ceramic Transactions, Nucleation and Crystallization in Liquids and Glasses* (Ref. [4]).
[43] J. D. Honeycutt and H. C. Anderson, J. Phys. Chem. **90**, 1585 (1986).
[44] J.-X. Yang, H. Gould, and W. Klein, Phys. Rev. Lett. **60**, 2665 (1988).
[45] W. Klein and F. Leyvraz, Phys. Rev. Lett. **57**, 2845 (1986).
[46] P. R. ten Wolde, M. J. Ruiz-Montero, and D. Frenkel, Phys. Rev. Lett. **75**, 2714 (1995).